SCATSAT-1 wind products for tropical cyclone monitoring, prediction and surface wind structure analysis

Neeru Jaiswal*, Prashant Kumar and C. M. Kishtawal

Atmospheric Sciences Division, Atmospheric and Oceanic Sciences Group, Earth, Ocean, Atmosphere, Planetary Sciences and Applications Area, Space Applications Centre (ISRO), Ahmedabad 380 015, India

The present study discusses the application of near real-time ocean surface wind vectors retrieved from scatterometer instrument, on-board Indian polar satellite SCATSAT-1, for tropical cyclone (TC) analysis and prediction. The real-time tropical cyclogenesis prediction of cyclonic activities in the North Indian Ocean basin has been presented using SCATSAT-1 wind data. The study also demonstrates the utility of high-resolution surface wind products of the scatterometer in monitoring mesoscale-level features of TCs for centre determination, size estimation and analysis of asymmetric wind radii. Impact of SCATSAT-1 winds for TC prediction using numerical weather prediction model has also been discussed. The shortcomings of ocean surface wind observations from space-based scatterometers are addressed, in addition to the sensor requirements for future satellite missions.

Keywords: Cyclogenesis, scatterometer, tropical cyclone, wind structure.

Introduction

TROPICAL CYCLONES (TCs) are warm-core, low-pressure, intense, synoptic-scale weather systems associated with strong swirling winds, intense clouds, storm surges and heavy precipitation. These systems form in the ocean depending on the presence of favourable environmental conditions like warm sea surface temperature (SST) (>27°C up to 15 m depth), low to moderate wind shear (10–15 kn), high humidity and vertical instability by drawing energy from the ocean[1]. When these systems approach towards the land, they cause large-scale destruction to life and property over the coastal regions. In the North Indian Ocean (NIO) region comprising Bay of Bengal (BoB) and Arabian Sea (AS), on an average 4–5 TCs form annually, during pre-monsoon (April–June) and post monsoon (October–December) months. India, with an extensive coastline, is vulnerable to meteorological disasters like TCs[2,3]. The advance and accurate prediction of TCs is highly important to mitigate the disastrous impact of land-approaching systems. India Meteorological Department (IMD), New Delhi is the official Regional Specialized Meteorological Centre (RSMC) in the NIO region for providing advisories during cyclones. Joint Typhoon Warning Centre (JTWC) in Hawaii, Unites States, also provide TC warning for this region. In addition to track and intensity, JTWC provides an ensemble of parameters describing the structure of surface wind fields in TCs as part of its TC advisory and warning process. These include the radius of maximum wind (R_{max}) and the maximum radial extent of critical wind speed thresholds of 34, 50 and 64 kn winds in four geographic quadrants (i.e. in the northeast ($Q1$), southeast ($Q2$), southwest ($Q3$) and northwest ($Q4$) directions). The quadrant wind information is used in numerical weather prediction (NWP) models for generating synthetic vortex that helps in improving the track and intensity forecasts[4], and in the storm-surge prediction models, to create wind stress for predicting storm surge[5].

TCs form in the open ocean where the network of *in situ* observations is sparse; thus satellite data are a major source of information. Satellite observations provide useful data to study the development, propagation, intensification and to infer structural parameters of TCs. The conventional satellite observations from satellite-borne radiometers in visible and infrared channels are limited to observing upper regions of the storms due to widespread cloud-cover; however, microwave measurements can penetrate within the clouds and provide surface parameters with good accuracies.

Scatterometers on-board satellites are among such instruments that have a capability of measuring both wind speed and wind direction over the ocean surface. Scatterometer, a microwave radar system, sends microwave pulses to the earth's surface and measures the backscattered power. The backscatter is largely determined by roughness of the surface, over the ocean, due to small centimetre-scale waves caused by friction with ocean winds. The backscatter depends not only on the magnitude of wind stress but also on wind direction relative to the direction of radar beam (azimuth angle). The relationship between backscatter power and wind speed is

*For correspondence. (e-mail: neerujaiswal@gmail.com)

governed by a geophysical model function (GMF). Ground processing of $\sigma 0$ measurements permits inversion of GMF to estimate wind from backscatter measurements[6].

Several generations of wind scatterometers have been flown in space by the National Aeronautics and Space Administration (NASA), USA; European Space Agency (ESA), France and the National Space Development Agency (NASDA) of Japan, with continuous improvement to the coverage and spatial resolution of ocean surface wind vectors[7]. In 1978, the first operational wind scatterometer, SEASAT (SASS), with a fan-beam system operating at Ku-band (14 GHz) was launched. In 1991, ESA launched the European Remote-Sensing Satellite (ERS-1) Advanced Microwave Instrument (AMI) scatterometer, followed by the ERS-2 AMI scatterometer in 1995, with fan-beam system operated at C-band (5.6 GHz). The Ku-band is more sensitive to wind variation at low winds, but is more subjective to rain contamination. In 1996, NASA launched the NASA Scatterometer (NSCAT), a Ku-band fan-beam system and in 1999, the first scanning scatterometer 'SeaWinds' on QuikSCAT, operated at Ku-band. ESA and European Organisation for the Exploitation of Meteorological Satellites (EUMETSAT) launched the first C-band advanced scatterometer (ASCAT) in 2006 on-board Metop-A. In 2009, the Indian Space Research Organisation (ISRO), launched a Ku-band scatterometer on Oceansat-2 satellite (OSCAT). In 2014, OSCAT stopped working and thereafter, ISRO launched its second Ku-band scatterometer SCATSAT-1 on September 2016, which is currently active and providing wind vector observations over the global oceanic basins.

Scatterometer wind vectors are retrieved at standard resolution of 25 and 50 km, which are derived from normalized backscattered power, returned from an ellipsoidal instantaneous antenna footprint. The standard products limit the interpretation of the scatterometer signals for mesoscale events, as strong gradients of the surface wind, existing at scales of a few kilometres are smoothed in the measured features such as the TC centre position, intensity, location of wind maxima, etc.[8]. Further enhancement of the resolution of wind products (~6 or 12.5 km) can be achieved by advanced approaches like dividing the antenna footprint into smaller, contiguous 'slices' using satellite on-board filtering[9,10]. These wind products of different resolution are used in a variety of atmospheric and oceanic applications[11,12]. However, the present study is limited to discussion regarding application of scatterometer data for TC studies. The improvement in TC track and intensity predictions by assimilating scatterometer data in NWP models has been shown by many researchers[13–22]. Other than NWP applications, scatterometer-derived surface wind measurements are used to resolve mesoscale features within TCs like centre, size, wind asymmetries, etc. High-resolution wind vectors retrieved from the scatterometer have been reported in the literature, to resolve the inner core features of TCs[23], pressure field near a TC[24] and climatology of TC size[25–28]. These products have been used to produce composites of TC surface wind distributions relative to vertical wind shear and storm motion directions in each TC-prone basin and various TC intensity stages[29]. The surface winds derived from the scatterometer have also been used for the 'early detection' of TCs[30–33].

The above studies concluded that information on surface wind patterns in TCs is of great importance for understanding and forecasting their formation and evolution. Satellite-based surface wind analysis is useful for surface wind field monitoring of TCs[34]. Observation by scatterometer provides a unique view of the surface wind patterns in the outer/inner core of TCs. Here we discuss the application of scatterometer on-board Indian satellite SCATSAT-1 for TC monitoring, prediction and wind structure analysis.

Study area and datasets

The study area of the present work includes the NIO region, which includes the BoB and AS. The datasets used are discussed below.

Scatterometer data

SCATSAT-1 satellite was launched on September 2016, as a follow-on mission of OSCAT which had stopped working in the February 2014. SCATSAT-1 carries a Ku-band pencil-beam scatterometer, which is an active microwave sensor at 13.515 GHz providing a ground resolution cell of size 50 km × 50 km. It conically scans the ground surface by generating two beams, the inner beam and the outer beam that are configured in horizontal and vertical polarization respectively, for both transmit and receive modes. It covers a continuous swath of 1400 km for the inner beam and 1840 km for the outer beam. SCATSAT-1 provides 90% coverage of the global oceans within a day. SCATSAT-1 data are available in real-time through the SAC-ISRO website (www.mosdac.gov.in). The wind data includes the standard products of 50 km × 50 km, 25 km × 25 km and high-resolution products of 6.5 km spatial resolution.

Cyclone best track data

Six named TCs were formed in the NIO, since the launch of SCATSAT-1 (i.e. during September 2016–December 2017). The best track data of these TCs have been obtained from India Meteorological Department (IMD), New Delhi. Figure 1 shows IMD best track positions of these six TCs. TC structural parameters (R_{max} and Radius

of Outermost Closed Isobar (ROCI)) have been obtained from JTWC best track data archive.

Since the scatterometer is in the polar orbit, it provides one or maximum two passes over the BoB and AS regions in a day. The cyclone is a moving weather phenomenon; so it is possible that it may not be captured in a day in any of the ascending or descending passes. Moreover, if the system is over land, then also wind observations cannot be provided by the scatterometer. SCATSAT-1 may not provide full coverage over the system; there is a possibility of partial coverage observations. Due to the above limitations, there is the likelihood of missing wind observations over the low-pressure systems forming in the oceanic basins. This may affect the lead time of cyclogenesis prediction, or may miss the system as well. For wind structure estimation, only those passes can be considered that have full coverage over the cyclone.

Methodology

The present work discusses utilization of SCATSAT-1 data for various TC applications like tropical cyclogenesis prediction, centre identification, size determination, wind asymmetries analysis, etc.

Observational analysis of SCATSAT data

Tropical cyclogenesis prediction: The all-weather capability of a scatterometer provides surface wind fields over TCs, including the most intense and cloud-covered low pressure systems. Very few such low pressure systems turn into TCs. The present study discusses advance prediction of tropical cyclogenesis in the NIO using SCATSAT-1 L2B products of 25 km × 25 km spatial resolution. The wind field patterns retrieved in each pass of SCATSAT-1 over the BoB and AS region during the cyclone-active months of NIO (April–June, October–December) were matched with archived wind field pattern database of previously developed low pressure systems observed by the past scatterometers (QuikSCAT and OSAT), as discussed in Jaiswal and Kishtawal[32,33].

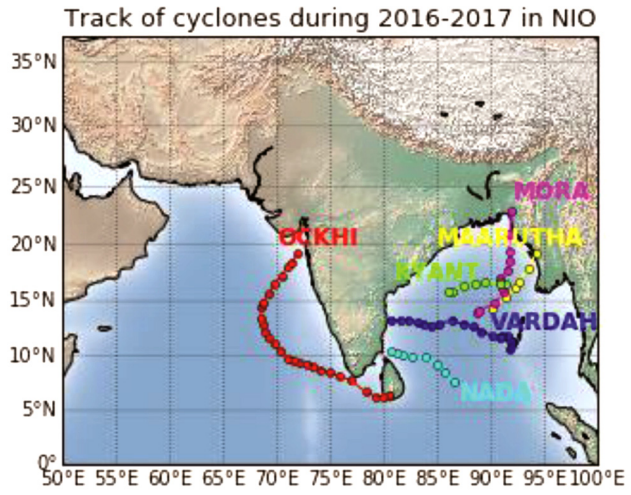

Figure 1. Track of tropical cyclones formed in the North Indian Ocean (NIO) during September 2016–December 2017.

The performance of cyclogenesis prediction using SCATSAT-1 data is assessed by estimating the verification skill scores, viz. probability of detection (POD), missing rate (MR), false alarm ratio, false alarm rate (FAR), bias, percentage correct (PC), correct non-occurrence (c-non), threat score (TS) or critical success index (CSI), and Heidke skill score (HSS) using the 2 × 2 contingency table. Estimation of these verification skill scores has been discussed by many authors[35,36]. The expressions for the above scores using the 2 × 2 contingency table (Table 1) are presented here.

$$\text{POD} = \frac{a}{a+b},$$

$$\text{MR} = \frac{c}{a+c},$$

$$\text{False alarm ratio} = \frac{b}{a+b},$$

$$\text{FAR} = \frac{b}{b+d},$$

$$\text{c-non} = \frac{d}{b+d},$$

$$\text{TS or CSI} = \frac{a}{a+b+c},$$

$$\text{Bias } (B) = \frac{a+b}{a+c},$$

$$\text{PC} = \frac{a+d}{a+b+c+d},$$

$$\text{HSS} = \frac{2(ad-bc)}{(a+c)(c+d)+(a+b)(b+d)}.$$

The above expressions are used to estimate the various skill scores that provide guidance about the skill of the model or technique.

Table 1. Contingency table for tropical cyclogenesis detection during 2016–17 using SCATSAT-1 data in the North Indian Ocean

	Event observed	
Event forecast	Yes	No
Yes	$a = 67$	$b = 34$
No	$c = 0$	$d = 857$

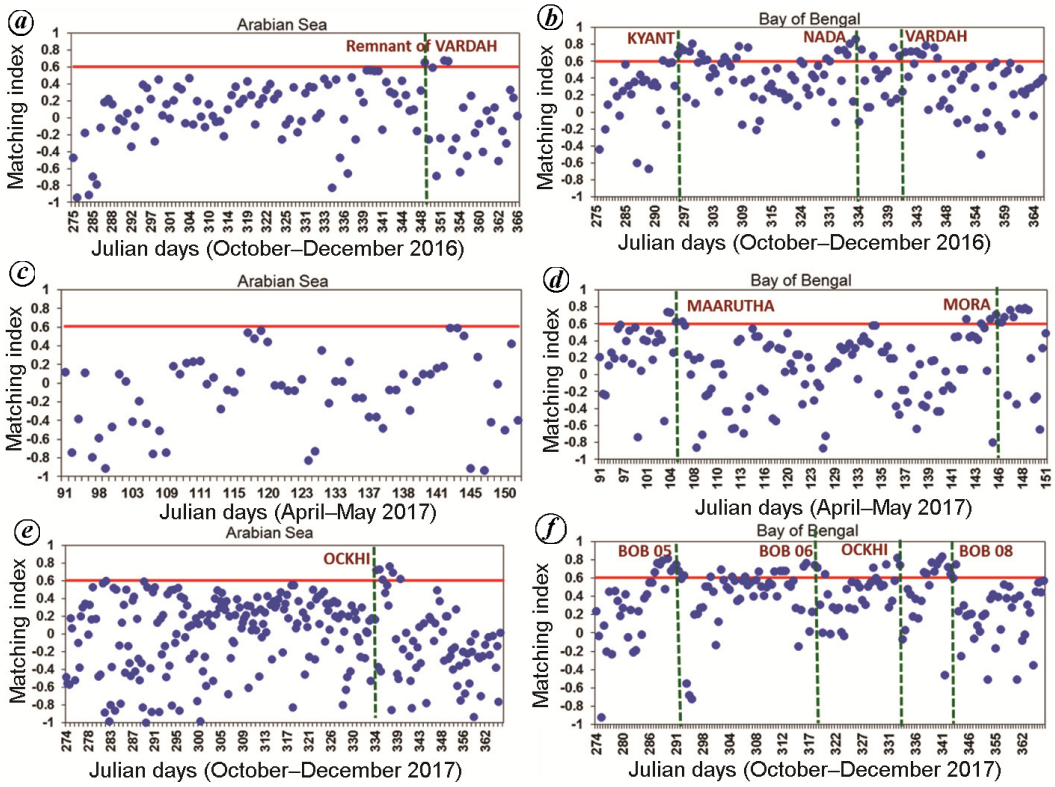

Figure 2 ***a–f.*** Wind pattern matching index obtained for all the SCATSAT-1 passes over the NIO region during cyclone-active months of 2016–17.

TC structural parameters estimation: High-resolution wind products of SCATSAT-1, which are available at 6.5 km resolution, were also explored in this study to assess their usefulness for TC structural parameters like geolocation, size and wind asymmetry. For this, the high-resolution winds obtained from each pass of SCATSAT-1 over all the six cyclonic systems have been analysed.

Estimation of cyclone geolocation: Accurate centre detection is a critical issue, because TC forecast models are highly sensitive to TC initial positions. During the development of low-pressure systems when their wind speed is in the category of depression, deep depression or cyclonic storm, the surface wind circulation is often not well-defined and may not be easily identified in visible or infrared satellite imagery. For such cases, the low-level centre estimated by the scatterometer derived wind field is useful. In the present work, centre of TC is estimated by identifying the centre of closed circulation which is an area of low wind speed in the core of the cyclonic vortex.

Estimation of cyclone size: ROCI, which is available from the best track archives, can be used as a TC size metric because it is well related to tangential wind speed profile of TCs[37]. Chavas and Emanuel[38] defined the size of TC as the radius of vanishing winds and created a climatology of TC size using QuikSCAT data of near-surface wind vectors. The size of TC is also defined as the radial extent of positive vorticity around the TC centre[25,39]. In this study, size of TCs is estimated by computing average distance between TC centre and 1×10^{-5} s^{-1} contour of relative vorticity[26,28,40]. TC size estimation based on the vorticity approach represents the outer radius of the cyclone beyond which it is assumed to have no deep convection.

Estimation of critical wind radii: For the wind radii analysis during TC warnings, four-quadrant radial extent of wind radii of gale force winds (34 kn), damaging force winds (50 kn) and hurricane force winds (64 kn) is important. Accurate estimates and forecasts of critical wind radii are also important as these values are used to determine the hazardous wind conditions associated with TCs; for example, wind speed probabilities[41], TC conditions of readiness and wave forecasting[42], and also in the NWP models[43]. SCATSAT-1 provides wind vectors in 1800 km wide swath, which is capable of providing full coverage over the TCs. Thus, it can be useful in determining the radial extent of 34 kn (17.5 m/s) wind speed, especially when the 34 kn wind radii extend outside the areas of convection. Due to rain contamination, there are negative biases in the high wind estimates; thus the radial extent of damaging force and hurricane force winds cannot be accurately estimated.

Assimilation of SCATSAT-1 retrieved wind vectors in NWP model

The Weather Research and Forecasting (WRF) model version 3.9, mainly developed for operational and research applications, is used in this study to assess the impact of SCATSAT-1 winds on TC track prediction. This model includes advanced numerical techniques, nesting options and various physics options for the treatment of convection and precipitation. The WRF model and assimilation methodology have been discussed in previous studies[44,45].

Results

The results of real-time tropical cyclogenesis prediction by analysing each of the SCATSAT-1 passes for TC active months of the NIO basin for 2016–17 (after the launch of SCATSAT-1) are presented in this section. The wind structure of TC has been analysed using high-resolution products of SCATSAT-1. As a case study, estimation of wind structural parameters of TC VARDAH (6–12 December 2016, NIO) has been discussed.

Tropical cyclogenesis prediction

Each day at least 3–4 passes of SCATSAT-1 are obtained over the NIO region covering the AS and BoB. Figure 2 *a–e* shows the wind pattern matching indices obtained for each pass of SCATSAT-1 over the AS and BoB, for October–December 2016, April–May 2017 and October–December 2017. The days are shown in Julian number in the *x*-axis and matching index values are shown in the *y*-axis. The red colour horizontal line shows the threshold limit (i.e. 0.6) of cyclogenesis for the NIO region. The values of matching indices exceeding 0.6, indicate TC formation alerts/or the existing cyclonic vortex. TC activity in the region is shown by vertical dotted lines on the Julian day when it was designated as a TC by IMD.

It can be seen from Figure 2 *a* and *b* that three systems, viz., KYANT, NADA and VARDAH (formation day is shown by vertical lines) were formed during October–December 2016 in the BoB region, which were predicted by the present technique and no false alarm was found. In the SCATSAT-1 pass of 14Z 18 October (Julian day 292), the matching index (0.61) was exceeding the threshold value. This system was classified as TC by IMD on 00Z 25 October (Julian day 299) and was named as 'TC KYANT'. The second TC in the post-monsoon season of 2016 was 'TC NADA', which was designated as a TC by IMD on 00Z 30 November (Julian day 335). The earliest detection of cyclogenesis of TC NADA was found on 03Z 27 November (Julian day 332), as the matching index (0.73) was exceeding the threshold limit. On 00Z 08 December, TC VARADAH was formed in the BoB region of NIO near the Andaman Sea. SCATSAT-1 pass showed the earliest cyclogenesis on 03Z 05 December, as the value of wind matching index was found to be 0.76. The matching indices computed during the days of April–May 2017, are shown in Figure 2 *c* and *d* for the AS and BoB regions respectively. The figure shows that during this period there was no cyclone in the AS and two systems (MAARUTHA and MORA) were formed in the BoB region, that were predicted before their formation and there were no false detections. MAARUTHA was designated as a TC by IMD on 18Z 15 April (Julian day 105) and was predicted by SCATSAT-1 on 03Z 14 April, i.e. 38 h prior to its formation as a TC. Cyclogenesis of TC Mora was predicted on 03Z 25 May (Julian day 145); however, it was designated as a TC by IMD on 06Z 28 May (Julian day 148). Similarly, the values of matching index obtained for the days of October–December 2017 are shown in Figure 2 *e* and *f* for the AS and BoB regions respectively. It can be seen from the figure that cyclone 'TC OCKHI' was formed in the NIO during this period. The earliest detection of cyclogenesis of TC OCKHI was done by SCATSAT-1 on 03Z 27 November; however, IMD designated the system as TC on 03Z 30 November (Julian day 334). The figure also shows that there were few false alarms in the BoB region during these months. The atmospheric and oceanic conditions were analysed during these false detections and it was found that due to the existence of high atmospheric wind shear conditions, the probable strengthening vortices could not intensify further and dissipated before developing into a TC.

Figure 3 shows the wind vectors retrieved by the SCATSAT-1 pass detecting the earliest cyclogenesis of the above-discussed TCs. The developing vortex has been marked by a square box. The value of wind pattern matching index (MI), and the date and time of SCATSAT-1 pass are also shown in the figure. The lead prediction time is also summarized. TC KYANT, NADA, VARDAH, MARUTHA and MORA were predicted 154, 69, 69, 38 and 75 h respectively, prior to their designation as a TC by IMD. The mean lead prediction time of the cyclogenesis prediction was computed as 79 h. It can be concluded that the scatterometers are well capable of providing wind observations to predict cyclogenesis in advance; however, the lead time of prediction is highly dependent on the coverage over the system. Since these instruments are deployed on the satellites orbiting in the polar orbits, only one or two observations are possible over the system which limits its temporal resolution.

All the SCATSAT-1 passes (958) over the NIO basin during the cyclone-active months have been analysed during 2016–17 for tropical cyclogenesis prediction. The cyclogenesis prediction skill of the technique using SCATSAT-1 data was assessed by estimating the forecast verification scores of the dichotomous (yes–no) events contingency table. Table 1 shows the contingency table for tropical cyclogenesis detection during 2016–17 using

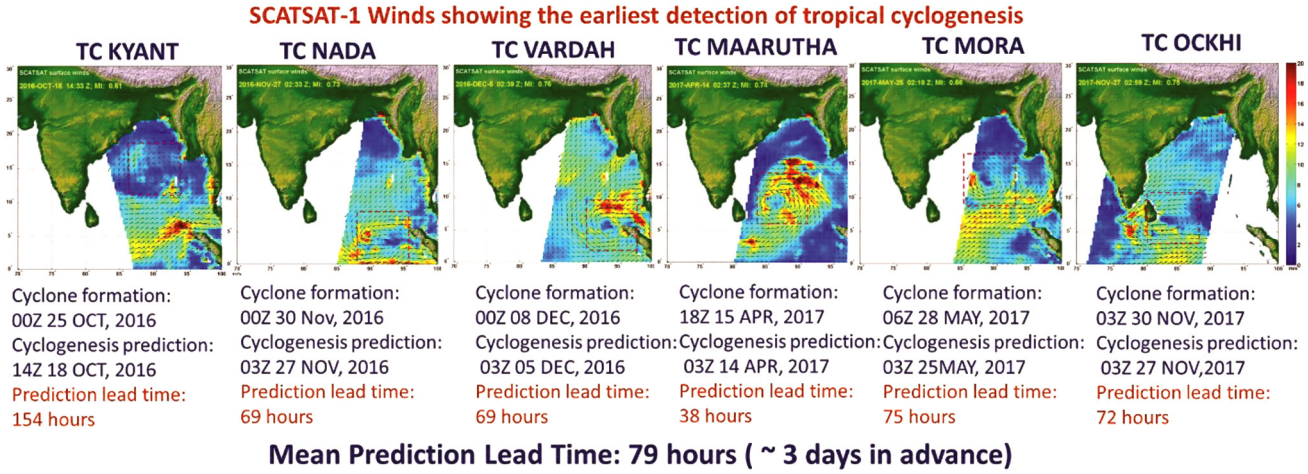

Figure 3. SCATSAT-1 wind vectors showing the earliest cyclogenesis of TCs formed in the NIO during 2016–17.

SCATSAT-1 data the NIO region. Based on this table, the POD or hit rate of cyclogenesis detection was computed as 1.0 and the missing rate was 0. This means that all the cyclones formed were predicted in advance, before these systems were designated as TCs by operational agencies. However, the false alarm ratio and rate were found to be 0.34 and 0.04 respectively. The value of bias was obtained as 1.51, which shows over-prediction of genesis event. While c-non was 0.96, PC was 0.97. TS or CSI and HSS were computed as 0.66 and 0.78 respectively. The values of CSI and HSS for NIO show a good forecasting skill.

Tropical cyclone structure parameters

The high-resolution wind products (~6 km) from scatterometers can be used to estimate the cyclone structural parameters like centre, size, V_{max}, R_{max}, critical wind radii, etc. As a case study, the structural parameters estimated using SCATSAT-1 high-resolution wind products (L4HW products) for TC VARDAH are discussed here. SCATSAT-1 provided six full coverages for TC VARDAH over its different intensity stages during 7–12 December 2016. For all these passes, the high-resolution wind product was processed and wind fields in the inner core region of TC were analysed. Figure 4 shows the geolocation (marked with '+' sign) estimated for all these passes of TC VARDAH. The geolocation estimated by surface wind observations can be considered as the most accurate position of the TC, and it can be used to correct the biases obtained during the centre estimated by the thermal infrared images from geo-stationary satellites. The results of centre estimation of TC VARDAH using high-resolution wind products are presented here. These values have been compared with IMD best track and JTWC best track data. The cyclone positions at the time of SCATSAT-1 pass have been computed in the three hourly IMD best track and six hourly JTWC best track data using linear interpolation. The mean difference between the cyclone positions estimated using SCATSAT-1 data with IMD and JTWC best track data was found to be 73 and 47 km respectively.

The size of TC VARDAH has been estimated by computing the mean distance of 1×10^{-5} s^{-1} vorticity contour as discussed earlier in the text. The values obtained were compared with the JTWC best track ROCI values for the nearest best track time and shown in Figure 4 for all the six SCATSAT-1 passes. It can be seen that values of size based on the vorticity approach are comparable with the JTWC ROCI estimates. The mean value of TC size estimated by SCATSAT-1 data was 344 km; however, the mean value of ROCI for these cases was 375 km. The mean difference between the JTWC ROCI and the estimated TC size for the above six cases was found to be 50 km. The global mean value of TC size was estimated as 423 km (ref. 38). The present analysis shows that TC VARDAH was a cyclone of smaller size compared to global mean size values. Its size was maximum during its developing stage (363 km) and minimum (297 km) when it attained its maximum intensity (80 kn).

The radial wind profile of TC VARDAH for the above six passes was analysed and the radial extent of winds reaching 34 kn (17 m/s) was computed in four quadrants. Figure 5 *a* shows the values obtained for all the passes over TC VARDAH in the northeast, northwest, southwest and southeast quadrants (expressed as *R*1, *R*2, *R*3 and *R*4 respectively). These values have been presented in Table 2 along with the JTWC best track estimated 34 kn wind radial estimates for nearly similar time. It can be seen that on 0330 Z 7 December 2016, only the estimate of *R*1 is given. This is because the cyclone was weak during this time and maximum wind speed in the other quadrants was less than 34 kn. The unestimated values are presented by '999' in the table. The system is in depression stage with maximum sustained wind as 25 kn at that time.

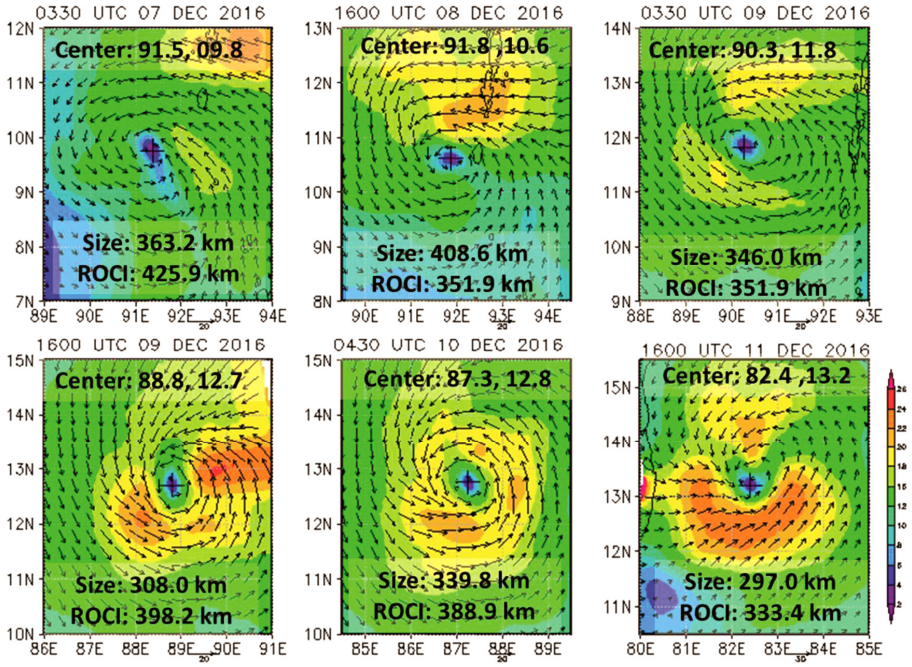

Figure 4. SCATSAT-1 wind observations over TC VARDAH during its genesis and intensification with its geolocation. The centre estimated by SCATSAT-1 is shown with the '+' mark. The wind vector arrows are down-sampled to increase visibility.

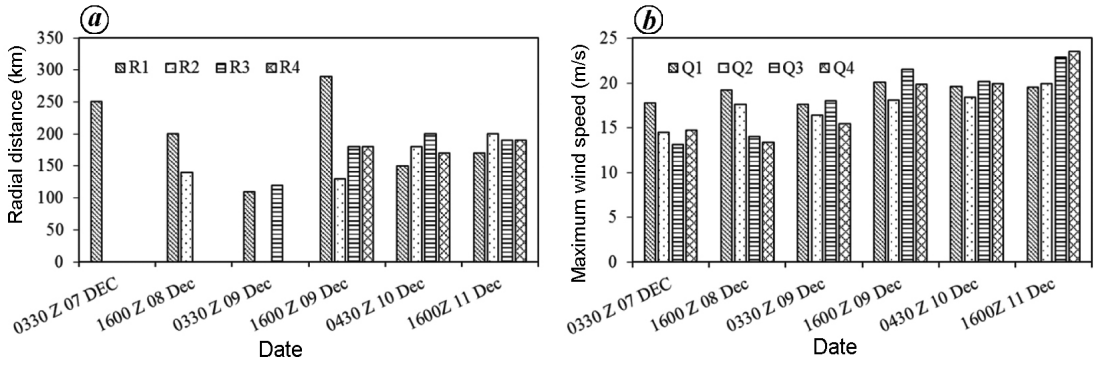

Figure 5. ***a***, Gale force wind radii estimates. ***b***, Quadrant wind distribution of TC VARDAH using SCATSAT-1 high-resolution wind products.

The winds estimated by the scatterometers are contaminated with rainfall over the low-pressure system; thus, there are some biases in wind speed estimations. Earlier studies have documented that values of radial extent of 34 kn winds increase with increase in intensification of TCs in all the quadrants in general[34]. However, in the case of TC VARDAH, no association of TC intensity and radial extent of the outer 34 kn wind is found in all four quadrants.

Winds vary greatly in all directions of a storm. The distribution of wind fields in all quadrants shows the asymmetric behaviour of wind pattern (Figure 5 *b*). These winds in the four quadrants indicate the greatest extent of winds anywhere in those quadrants of a TC. These estimates are highly useful in risk assessment during landfall of TCs. In the case of TC VARDAH, the scatterometer pass shows that just before landfall the winds are higher in the third (SW) and fourth (SE) quadrants. So, if these sectors of cyclones hit the land, disaster due to TC will be relatively higher.

Assimilation of SCATSAT-1 retrieved wind vectors in NWP model

The WRF model version 3.9 was used in this study to assess the impact of SCATSAT-1 winds on TC track prediction. As a case study the results for TC OCKHI are presented here. Two parallel experiments were performed with ('SCAT') and without ('CNT') assimilation of SCATSAT-1 retrieved winds, in addition to conventional and other satellite observations, using three-dimensional variational (3D-Var) data assimilation method during 3–6 December 2017. The selections of model physics are broadly adopted from Kumar and Varma[46]. Details of 3D-Var data assimilation are given in the literature[45–47]. The

Table 2. Gale force wind radii estimates in all four quadrants

Date	Tropical cyclone intensity (kn)	Radial extent of outer 34 kn wind (km)			
		*R*1 (NE)	*R*2 (NW)	*R*3 (SW)	*R*4 (SE)
0330 07 December	25	250 (999)*	999 (999)	999 (999)	999 (999)
1600 08 December	40	200 (204)	140 (148)	999 (111)	999 (167)
0330 09 December	45	110 (111)	999 (111)	120 (111)	999 (111)
1600 09 December	50	290 (185)	130 (93)	180 (167)	180 (222)
0430 10 December	55	150 (195)	180 (130)	200 (204)	170 (130)
1600 11 December	70	170 (185)	200 (130)	190 (130)	190 (185)

*Values in brackets are the best track estimates of Joint Typhoon Warning Centre (JTWC) for the nearest time of SCATSAT-1 pass. The unestimated values are represented by '999'.

National Center of Environmental Prediction (NCEP) final analysis ($0.25° \times 0.25°$ spatial resolution) was used to prepare the model lateral boundary conditions for both experiments. The 6 h WRF model forecast from 0000, which was valid at 0600 UTC 3 December 2017, was used as the first guess for cyclic assimilation from 0600 to 1800 UTC. This procedure was adopted instead of directly using the NCEP analysis as the first guess. In this study, observation errors are assumed uncorrelated in space and time, and as a diagonal matrix. The diagonal elements of these covariance matrices are variances of the SCATSAT-1 observation error and assumed constant in space and time. The standard deviations for SCATSAT-1 wind speed and direction are 1.6 ms^{-1} and 20° respectively.

Figure 6 *a* shows the simulated cyclone track from both experiments along with the IMD-observed best track. Variational data assimilation modified the initial position of SCAT experiment in comparison with CNT experiment. Minute changes were found in the first 24 h track forecasts from 1800 UTC 3 December 2017 (Figure 6 *b*). Further, SCATSAT-1 based experiment was performed closer to IMD best track compared to CNT experiment. It is interesting to note that a temporal error was observed in the CNT experiment, which improved after assimilation of SCATSAT-1 winds. Results suggest that mean track error reduces from 175 km in CNT run to 115 km in SCAT run after the assimilation of SCATSAT-1 winds. This mean track error reduction is substantial when considering model predictions beyond 24 h (reduced from 290 km in CNT run to 170 km in SCAT run). Moreover, model-simulated mean ROCI, R_{max} and gale force wind radii in all four quadrants were compared with JTWC best track data (Table 3). Results suggest that R_{max} predictions are improved with the assimilation of SCATSAT-1 winds for *R*34 and *R*50, whereas no significant changes are found in ROCI predictions. Overall, the results suggest that assimilation of SCATSAT-1 winds improves track prediction with less impact on cyclone structure analysis.

Discussion and conclusions

The present study discusses application of scatterometer-retrieved wind fields for TC monitoring prediction and structural analysis. The utilization of wind products of SCATSAT-1 for tropical cyclogenesis prediction of TCs in the NIO basin is highlighted. The results show that the SCATSAT-1 data predict the advanced cyclogenesis of TCs formed in the NIO basin with the lead prediction time of three days (~79 h). There are a few false alarms, which were corrected after including the atmospheric wind shear conditions. Thus, the combination of surface wind observed by SCATSAT-1 and atmospheric wind shear provides a reasonably good possibility of cyclogenesis prediction.

The high-resolution products were also generated from SCATSAT-1 σ^0 observations. These products were found to be highly useful for TC surface wind structural analysis, as shown in the study for TC VARDAH. The six passes of SCATSAT-1 over the full coverage of TC VARDAH during different intensity stages of its duration have been analysed and the results showing the estimates of TC geolocation, size, critical wind radii and quadrant wind distribution are discussed. The cyclone prediction models are highly sensitive to initial conditions like TC centre and size. The estimates of TC geolocation and size parameter presented in this study can be used for this purpose. The centre values estimated using SCATSAT-1 wind fields were matched with the best track estimates from IMD and found to be in good proximity. The size of TC was estimated using the vorticity approach and found to be comparable with respect to the JTWC ROCI values. However, more data are required for analysing the size characteristics of TC in the NIO basin.

The high-resolution wind products were also used and have been shown for analysing wind asymmetry in the TCs. The values of gale force wind radii (radius of 34 kn winds) in the four quadrants have been estimated and presented. The results show how wind asymmetry varies during different intensity stages of TC VARDAH, and the existence of gale force winds closer to the centre for comparatively intense cyclone stages. The maximum wind speed existing in all the four quadrant has also been shown for TC VARDAH. These products are useful to assess the extent of the most dangerous area of the existing cyclone and thus maybe helpful during TC risk analysis. The assimilation of SCATSAT-1 data in the WRF

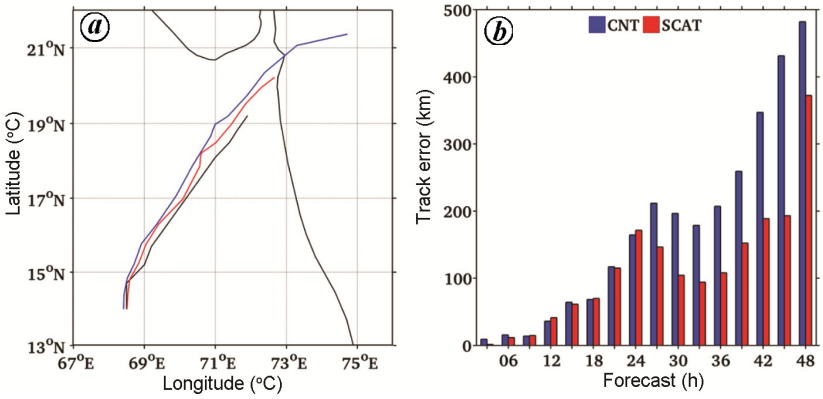

Figure 6. ***a***, Track prediction from India Meteorological Department (IMD) best track (black), and CNT (blue) and SCAT (red) experiment from 1800 UTC 3 December 2017 to 1800 UTC 5 December 2017. ***b***, Track error (km) for CNT and SCAT runs against IMD best track observations.

Table 3. Mean radius of outermost closed isobar (ROCI), R_{max} and gale force wind radii in all four quadrants for JTWC data, and CNT and SCAT simulations using weather research and forecast (WRF) model

JTWC observation/WRF simulation		ROCI (kn)	R_{max} (kn)	Radial extent of outer wind (km)			
				*R*1	*R*2	*R*3	*R*4
34 kn	JTWC	192	18	128	119	92	111
	CNT	297	12	87	78	71	77
	SCAT	295	16	101	73	66	85
50 kn	JTWC	190	17	65	65	45	55
	CNT	298	13	45	43	36	43
	SCAT	297	16	50	45	42	42
64 kn	JTWC	188	16	36	35	24	29
	CNT	296	14	34	34	32	32
	SCAT	298	14	29	33	32	34

model has been performed and improvement in the TC track prediction has been demonstrated in the case of TC OCKHI. Results suggest noteworthy improvements in track prediction beyond 24 h forecasts.

Scatterometer wind data obtained from satellites like SCATSAT-1 help in providing the large surface observations over global oceans. These observations have been widely used by researchers, and have resulted in improved analyses of surface features, better definition of high wind areas and improved forecasts of high-wind events. Scatterometer satellites, being flown on polar orbits, have a limitation that they provide one or two passes in a day over the low-pressure systems developing/or existing in the oceans. Sometimes they miss the coverage or provide partial coverage over cyclonic systems. This affects the lead prediction time of cyclogenesis. Thus, for higher lead prediction time and more frequent observations of the cyclonic vortices, more scatterometers are required. Due to heavy rainfall during cyclonic systems, the wind estimates are rain-contaminated and the high wind estimation is also a limitation. For wider applications, the rain sensitivity and high wind sensitivity of scatterometers should be addressed. This may be done using the cross-polarization and dual frequency scatterometer. A radiometer can also be flown along with the scatterometer, which can be used to correct the estimations during rainy cases.

1. Gray, W. M., Global view of the origin of tropical disturbances and storms. *Mon. Weather Rev.*, 1968, **96**(10), 669–700.
2. Mohapatra, M., Mandal, G. S., Bandyopadhyay, B. K., Tyagi, A. and Mohanty, U. C., Classification of cyclone hazard prone districts of India. *Nat. Hazards*, 2012, **63**, 1601–1620.
3. Mohapatra, M., Bandyopadhyay, B. K. and Tyagi, A., Best track parameters of tropical cyclones over the North Indian Ocean: a review. *Nat. Hazards*, 2012, **63**, 1285–1317.
4. Chourasia, M., Asrit, R. G. and George, J. P., Impact of cyclone bogussing and regional assimilation on tropical cyclone track and intensity prediction. *Mausam*, 2013, **64**, 135–148.
5. Dube, S. K., Poulose, J. and Rao, A. D., Numerical simulation of storm surge associated with severe cyclonic storms in the Bay of Bengal during 2008–11. *Mausam*, 2013, **64**(1), 193–202.
6. Gohil, B. S., Sikhakolli, R. and Gangwar, R. K., Development of geophysicsl model functions for Oceansat-2 scatterometer. *IEEE GRSL*, 2013, **10**(2), 377–380.
7. Liu, W. T., Hu, H., Song, Y. T. and Tang, W., Improvement of scatterometer wind vectors – impact on hurricane and coastal studies. In Proceedings of WCRP/SCOR Workshop on Intercomparison and Validation of Ocean–Atmosphere Flux Fields. World Meteorological Organization – Publications WMO TD, 2001, 2001, pp. 197–200.
8. Quilfen, Y., Chapron, B., Elfouhaily, T., Katsaros, K. and Tourna, J., Observation of tropical cyclones by high-resolution scatterometry. *J. Geophys. Res.*, 1998, **103**, 7767–7786.

9. Tang, W., Liu, W. T. and Stiles, B. W., Evaluation of high-resolution ocean surface vector winds measured by QuikSCAT scatterometer in coastal regions. *IEEE Trans. Geosci. Remote Sensing*, 2004, **42**, 1762–1769.
10. Lindsley, R. D., Blodgett, J. R. and Long, D. G., Analysis and validation of high-resolution wind from ASCAT. *IEEE Trans. Geosci. Remote Sensing*, 2016, **54**, 5699–5711.
11. Chelton, D. B., Freilich, M. H., Sienkiewicz, J. M. and Ahn, J. M. V., On the use of QuikSCAT scatterometer measurements of surface winds for marine weather prediction. *Bull. Am. Meteorol. Soc.*, 2006, **134**, 2055–2071.
12. Brennan, M. J., Hennon, C. C. and Knabb, R. D., The operational use of QuikSCAT Ocean surface vector winds at the national hurricane center. *Weather Forecast.*, 2009, **24**, 621–645.
13. Stoffelen, A. and Cats, J. C., The impact of seasat-A scatterometer data on high-resolution analyses and forecasts: the development of the QEII storm. *Mon. Weather Rev*., 1991, **119**, 2794–2802.
14. Atlas, R., Hoffman, R. N., Leidner, S. M. and Sienkiewicz, J., The effects of marine winds from scatterometer data on weather analysis and forecasting. *Bull. Am. Meteorol. Soc*., 2001, **82**, 1965–1990.
15. Isaksen, L. and Janssen, P. A., Impact of ERS scatterometer winds in ECMWF's assimilation system. *Q. J. R. Meteorol. Soc*., 2004, **130**, 1793–1814.
16. Rambabu, G., QuikSCAT scatterometer wind data impact on tropical cyclone forecasts by a mesoscale model. *Mausam*, 2006, **57**, 141.
17. Singh, R., Kishtawal, C. M., Pal, P. K. and Joshi, P. C., Assimilation of the multisatellite data into the WRF model for track and intensity simulation of the Indian Ocean tropical cyclones. *Meteorol. Atmosph. Phys.*, 2011, **111**(3–4), 103–119.
18. Jung, B. J., Kim, H. M., Auligne, T., Zhang, X., Zhang, X. and Huang, X. Y., Adjoint derived observation impact using WRF in the western North Pacific. *Mon. Weather Rev.*, 2013, **141**, 4080–4097.
19. Prasad, S. V., Gupta, A. and Rajagopal, E. N., Impact of OSCAT surface wind data on T574L64 assimilation and forecasting system – a study involving tropical cyclone Thane. *Curr. Sci*., 2013, **104**, 627–631.
20. Greeshma, M. M., Srinivas, C. V., Naisu, C. V., Baskaran, R. and Venkatraman, B., Impact of local data assimilation on tropical cyclone predictions over the Bay of Bengal using the ARW model. *Annu. Geophys.*, 2015, **33**, 805–828.
21. Dodla, V. B., Srinivas, D., Dasari, H. P. and Gubbala, C. S., Prediction of tropical cyclone over North Indian Ocean using WRF model: sensitivity to scatterometer winds, ATOVS and ATMS radiances. *Proc. SPIE: Remote Sensing Model. Atmos., Oceans Interact VI*, 2016, **9882**, 988213.
22. Duan, B., Zhang, W., Yang, X., Dai, H. and Yu, Y., Assimilation of typhoon wind field retrieved from scatterometer and SAR based on the Huber norm quality control. *Remote Sensing*, 2017, **9**, 987.
23. Liu, W. T., Hu, H. and Yueh, S., Interplay between wind and rain observed in hurricane Floyd, *Trans. AGU*, 2000, **81**, 253–253.
24. Hsu, C. S. and Liu, W. T., Wind and pressure fields near tropical cyclone Oliver derived from scatterometer observations. *J. Geophys. Res.*, 1996, **101**, 17021–17027.
25. Liu, K. S. and Chan, J. C., Size of tropical cyclones as inferred from ERS-1 and ERS-2 data. *Mon. Weather Rev.*, 1999, **127**(12), 2992–3001.
26. Chan, K. T. and Chan, J. C., Size and strength of tropical cyclones as inferred from QuikSCAT data. *Mon. Weather Rev.*, 2012, **140**(3), 811–824.
27. Knaff, J. A., Longmore, S. P. and Molenar, D. A., An objective satellite-based tropical cyclone size climatology. *J. Climate*, 2014, **27**, 455–476.
28. Jaiswal, N., Ha, D. T. T. and Kishtawal, C. M., Estimation of size of tropical cyclones in the North Indian Ocean using Oceansat-2 scatterometer high-resolution wind products. *Theor. Appl. Climatol.*, 2019, **136**, 45–53.
29. Klotz, B. W. and Jiang, H., Global composites of surface wind speeds in tropical cyclones based on a 12 year scatterometer database, *Geophys. Res. Lett.*, 2016, **43**, 10480–10488.
30. Sharp, R. J., Bourassa, M. A. and O'Brien, J. J., Early detection of tropical cyclones using sea winds-derived vorticity. *Bull. Am. Meteorol. Soc.*, 2002, **83**, 879–889.
31. Hite, M. M., Bourassa, M. M., Cunningham, P., O'Brien, J. J. and Reasor, P. D., Vorticiy based detection of tropical cyclogenesis. *J. Appl. Meteorol. Climatol.*, 2007, **46**, 1214–1229.
32. Jaiswal, N. and Kishtawal, C. M., Prediction of tropical cyclogenesis using scatterometer data. *IEEE Trans. Geosci. Remote Sensing*, 2011, **49**, 4904–4909.
33. Jaiswal, N., Kishtawal, C. M. and Pal, P. K., Prediction of tropical cyclogenesis in North Indian Ocean using OSCAT data. *Meteorol. Atmos. Phys.*, 2013, **119**, 137–149.
34. Mohapatra, M. and Sharma, M., Characteristics of surface wind structure of tropical cyclones over the North Indian Ocean. *J. Earth Syst. Sci.*, 2015, **124**, 1573–1598.
35. Wilks, D. S., *Statistical Methods in the Atmospheric Sciences: An Introduction*. Academic Press, San Diego, California, 1995, 465.
36. Goyal, S., Mohapatra, M., Kumar, A., Dube, S. K., Rajendra, K. and Goswami, P., Validation of a satellite-based cyclogenesis technique over the North Indian Ocean. *J. Earth Syst. Sci.*, 2016, **125**, 1353–1363.
37. Miller, A. and Anthes, R., *Meteorology*, Merril Publishing, Columbus, 1985.
38. Chavas, D. R. and Emanuel, K. A., A QuikSCAT climatology of tropical cyclone size. *Geophys. Res. Lett.*, 2010, **37**(18), L18816.
39. Ahrens, C. D., *Essentials of Meteorology*, Wadsworth Publishing, Belmont, 1998, 2nd edn.
40. Chan, J. C. and Yip, C. K., Interannual variations of tropical cyclone size over the western North Pacific. *Geophys. Res. Lett.*, 2003, **30**(24), 2267.
41. DeMaria, M. *et al.*, Improvements to the operational tropical cyclone wind speed probability model. *Weather Forecast.*, 2013, **28**, 586–602.
42. Sampson, C. R., Wittmann, P. A. and Tolman, H. L., Consistent tropical cyclone wind and wave forecasts for the US Navy. *Weather Forecast.*, 2010, **25**, 1293–1306.
43. Bender, M. A., Ginis, I., Tuleya, R., Thomas, B. and Marchok, T., The operational GFDL coupled hurricane–ocean prediction system and summary of its performance. *Mon. Weather Rev.*, 2007, **135**, 3965–3989.
44. Singh, R., Kumar, P. and Pal, P. K., Assimilation of Oceansact-2 scatterometer derived surface winds in the weather research and forecasting model. *IEEE Trans. Geosci. Remote Sensing*, 2012, **50**(4), 1015–1021.
45. Kumar, P., Kishtawal, C. M. and Pal, P. K., Sensitivity analysis of high resolution Oceansat-2 scatterometer winds on Thane cyclone simulation. *Int. J. Remote Sensing*, 2014, **35**(23), 7927–7940.
46. Kumar, P. and Varma, A. K., Assimilation of INSAT-3D hydro estimator method retrieved for short range weather prediction. *Q. J. R. Meteorol. Soc.*, 2017, **143**, 384–394.
47. Kumar, P., Kishtawal, C. M. and Pal, P. K., Impact of ECMWF, NCEP, and NCMRWF global model analysis on the WRF model forecast over Indian region. *Theor. Appl. Climatol*., 2017, **127**, 143–151.

ACKNOWLEDGEMENTS. We thank the Director, SAC (ISRO), Ahmedabad and Deputy Director of EPSA, SAC. We acknowledge the Joint Typhoon Warning Centre and Regional Specialized Meteorological Centre for tropical cyclones over the North Indian Ocean, India Meteorological Department, New Delhi for providing best track data of tropical cyclones. The satellite observations of SCATSAT-1 were obtained from MOSDAC (www.mosdac.gov.in). We also thank the reviewers for their valuable suggestions.

doi: 10.18520/cs/v117/i6/983-992